nature portfolio

https://doi.org/10.1038/s41929-022-00796-1

Supplementary information

Atomically dispersed Pt and Fe sites and Pt–Fe nanoparticles for durable proton exchange membrane fuel cells

In the format provided by the authors and unedited

SUPPLEMENTARY INFORMATION

Atomically Dispersed Pt and Fe Sites and Pt-Fe Nanoparticles for Durable Proton Exchange Membrane Fuel Cells

Fei Xiao[1,11], Qi Wang[2,11], Gui-Liang Xu[3,11], Xueping Qin[1,11], Inhui Hwang[4], Cheng-Jun Sun[4], Min Liu[5], Wei Hua[6], Hsi-wen Wu[1], Shangqian Zhu[1], Jin-Cheng Li[1,7], Jian-Gan Wang[6], Yuanmin Zhu[2], Duojie Wu[2], Zidong Wei[8], Meng Gu[2,], Khalil Amine[3,9,*], Minhua Shao[1,7,10,*]*

[1]Department of Chemical and Biological Engineering, The Hong Kong University of Science and Technology, Clear Water Bay, Kowloon, Hong Kong

[2]Department of Materials Science and Engineering, Southern University of Science and Technology, Shenzhen, Guangdong 518055, China

[3]Chemical Sciences and Engineering Division, Argonne National Laboratory, Lemont, Illinois 60439, United States

[4]X-ray Science Division, Argonne National Laboratory, Lemont, Illinois 60439, United States

[5]College of Nuclear Science and Technology, University of South China, Hengyang 421001, China

[6]Department of Materials Science and Engineering, Northwestern Polytechnical University, Xi'an, Shaanxi 710071, China

[7]Fok Ying Tung Research Institute, The Hong Kong University of Science and Technology, Guangzhou, 518057, China

[8]College of Chemistry and Chemical Engineering, Chongqing University, Chongqing, 400044, China

[9]Materials Science and Engineering, Stanford University, Stanford, California 94309, United States

[10]Energy Institute, and Chinese National Engineering Research Center for Control & Treatment of Heavy Metal Pollution, The Hong Kong University of Science and Technology, Clear Water Bay, Kowloon, Hong Kong

[11]Equal contributions

*Corresponding authors

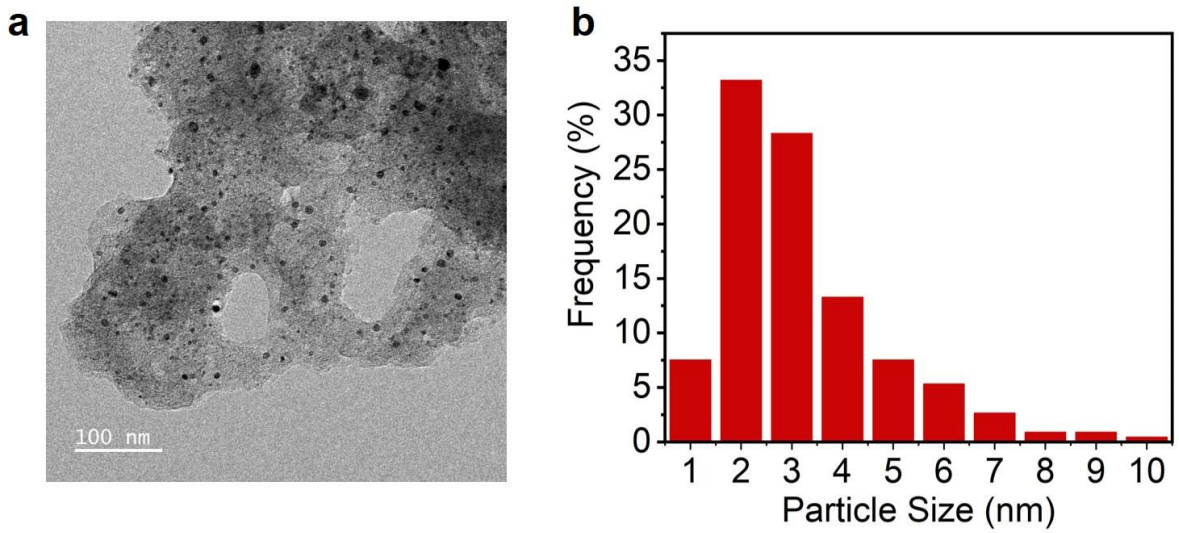

Supplementary Figure 1: (**a**) A typical TEM image for particle size survey. (**b**) Particle size distribution of Pt-Fe-N-C catalyst. The survey includes around 400 nanoparticles with clear boundaries.

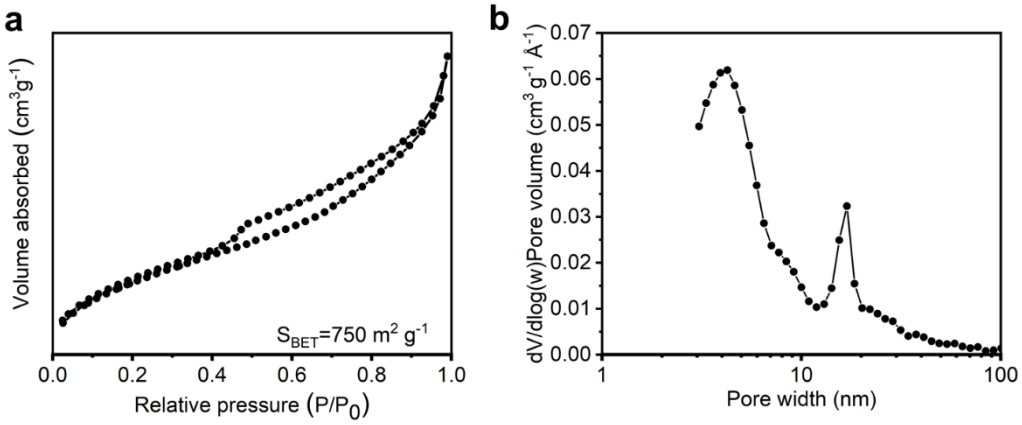

Supplementary Figure 2: (**a**)The nitrogen absorption isotherm and (**b**) pore volume size distribution of Pt-Fe-N-C catalyst.

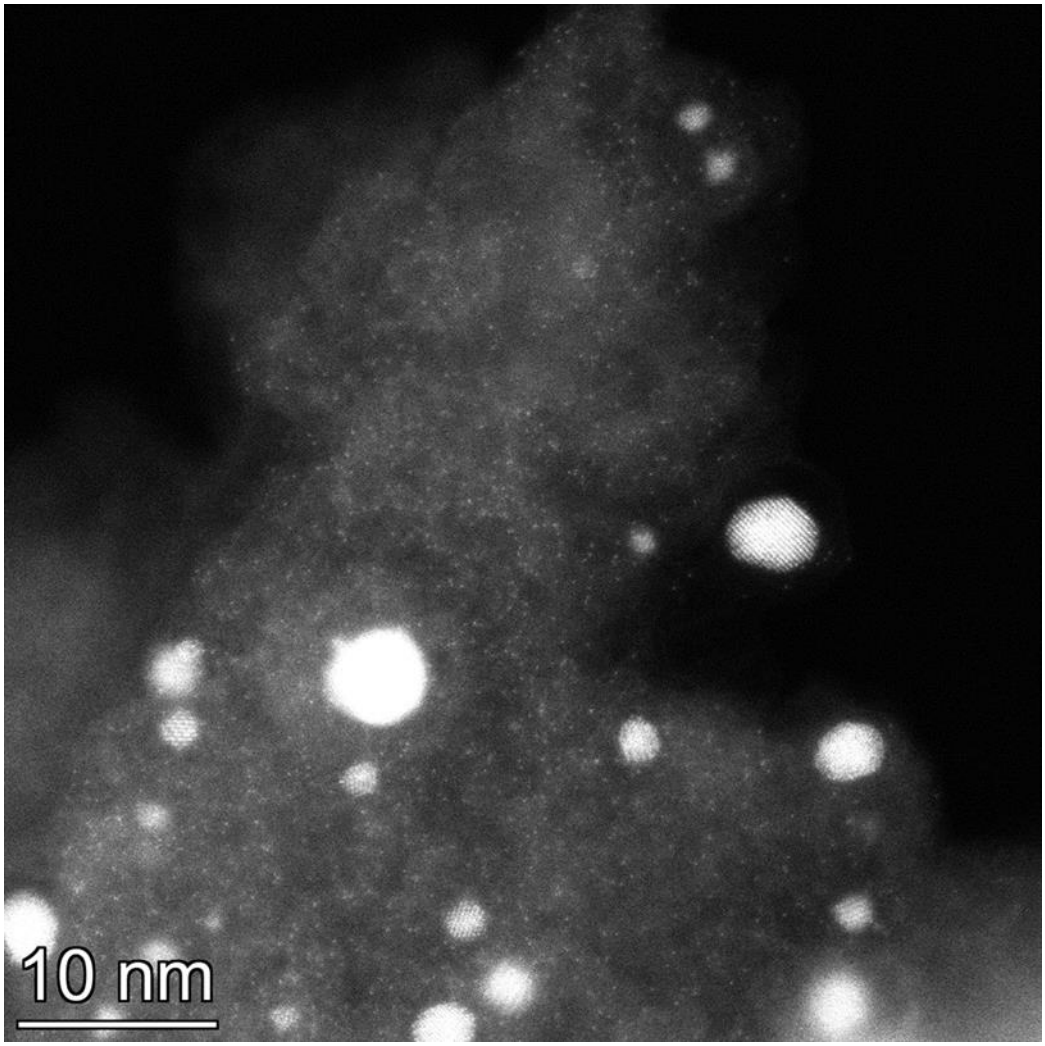

Supplementary Figure 3: HAADF-STEM image of Pt-Fe-N-C catalyst.

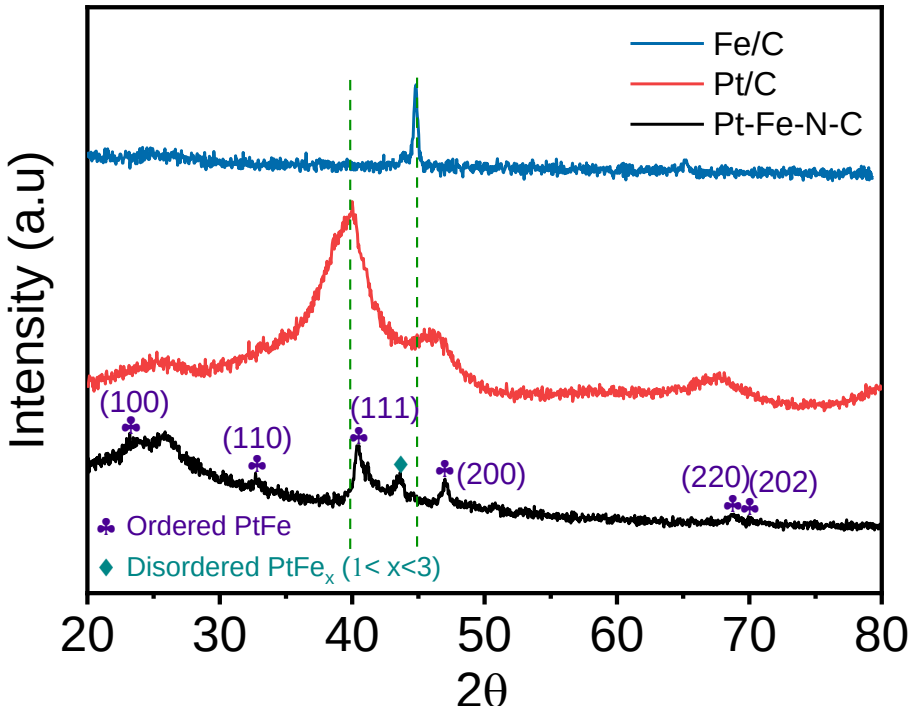

Supplementary Figure 4: XRD pattern for Pt-Fe-N-C (ordered PtFe (JCPDS #43-1359)) with the reference of Fe/C (JCPDS #6-0696) and Pt/C (JCPDS #4-0802).

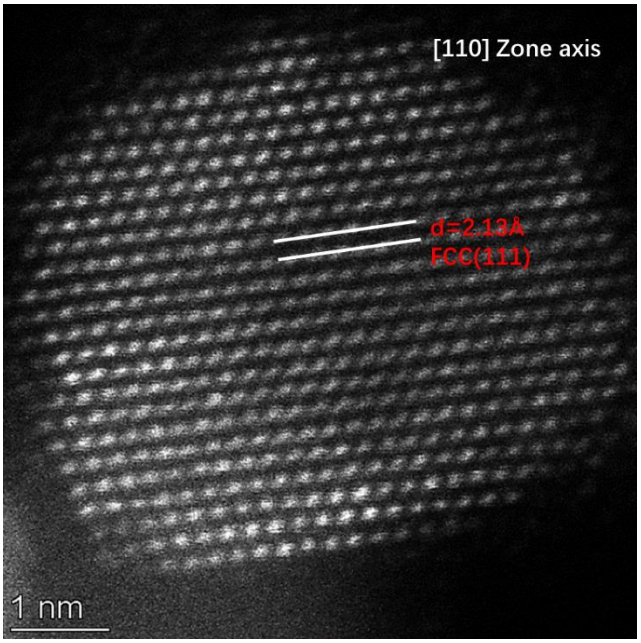

Supplementary Figure 5: HAADF-STEM image of a bigger particle along [110] zone axis. It has the lattice space of 2.13 Å (111) and is identified as disordered $PtFe_x$ ($1<x<3$).

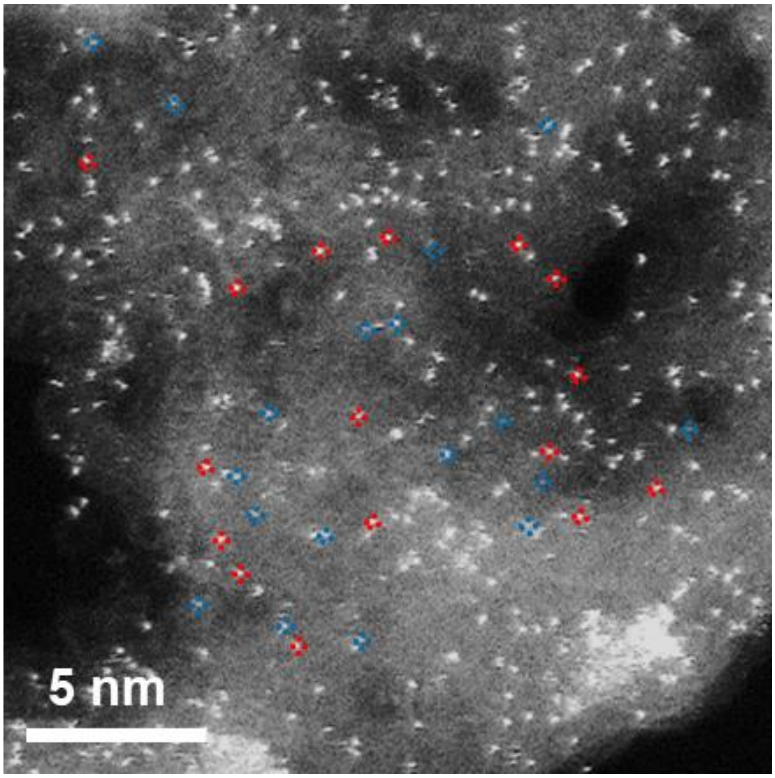

Supplementary Figure 6: HAADF-STEM image of "particle-free" carbon region in Pt-Fe-N-C catalyst, in which the blue and red dashed circles denote Fe and Pt single atoms, respectively.

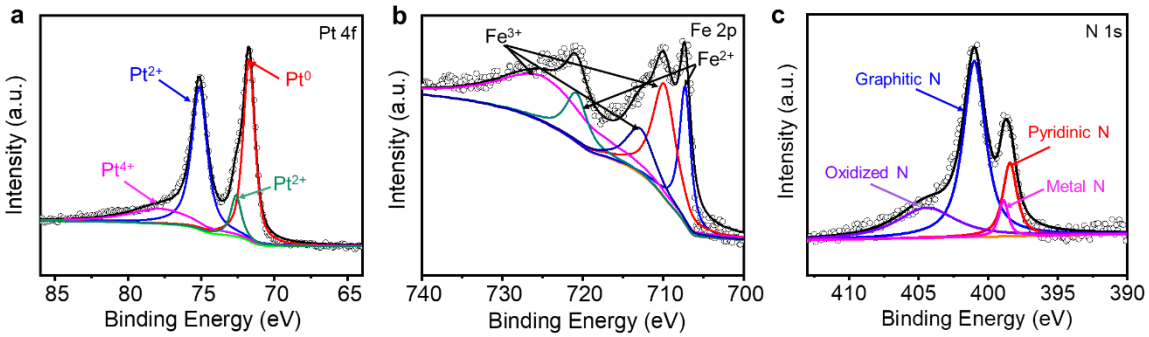

Supplementary Figure 7: XPS result for (**a**) Pt 4f, (**b**) Fe 2p and (**c**) N 1s spectra for Pt-Fe-N-C catalyst.

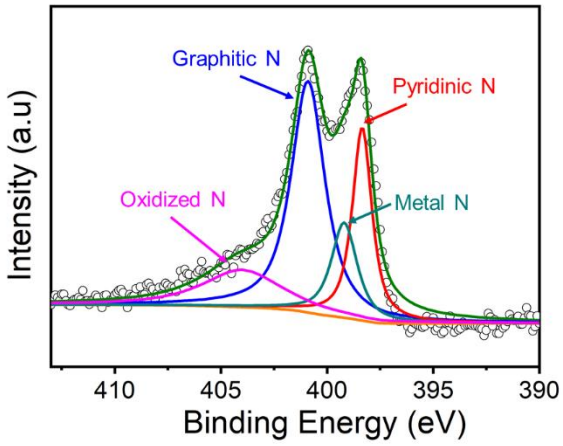

Supplementary Figure 8: XPS result for N 1s spectrum for Fe-N-C catalyst.[1]

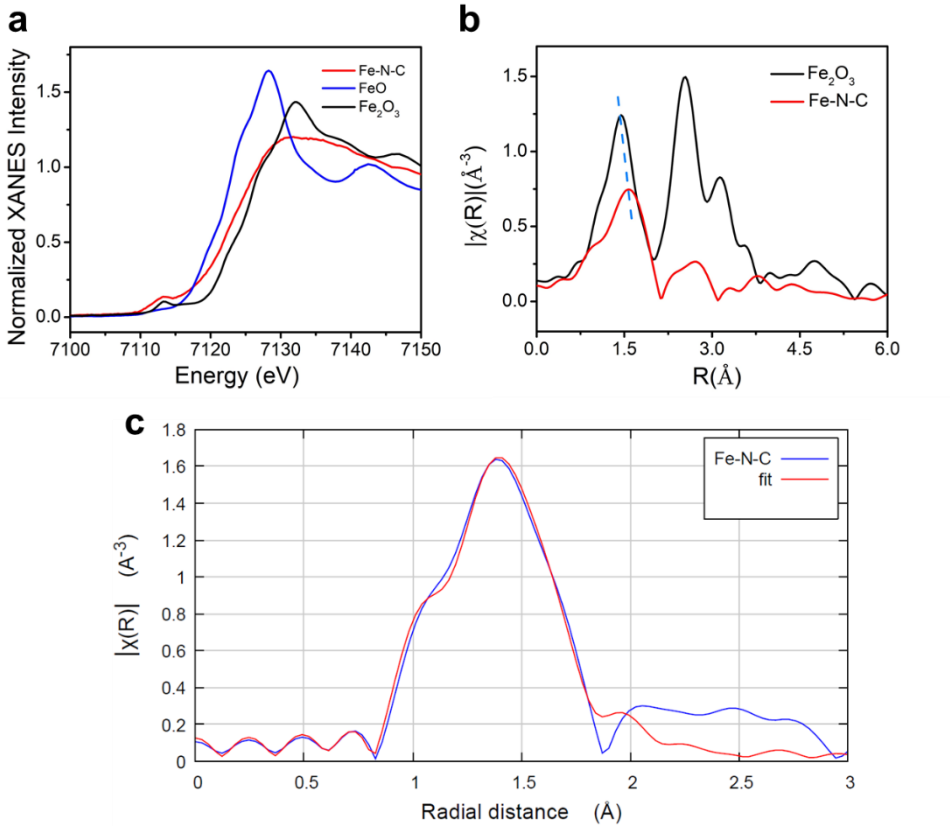

Supplementary Figure 9: Comparison of XAS spectra of Fe-N-C with Fe based references (red line for Fe-N-C catalyst, blue line for FeO, and black line for Fe_2O_3): (**a**) XANES spectra of Fe K-edge where the spectra are k^2 weighted and (**b**) Fourier transforms for EXAFS spectra of Fe K-edge where the spectra are k^3 weighted. A clear shift is indicated by a dashed blue line. (**c**) EXAFS fitting using Fe-N and Fe-O scattering paths for Fe-N-C. More details could be found in the literature.[1]

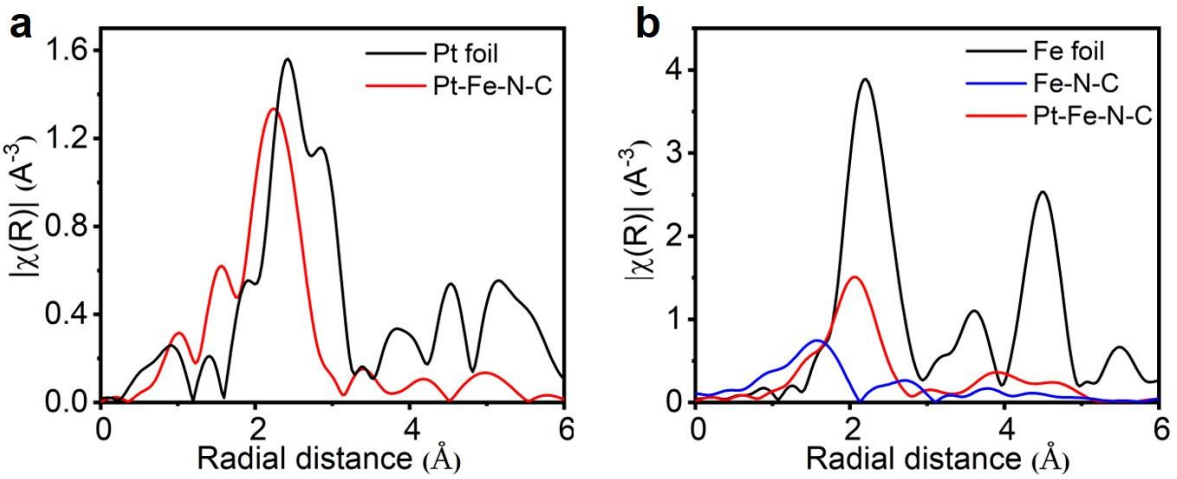

Supplementary Figure 10: Comparisons of FT-EXAFS spectra for (**a**) Pt L_3-edge and (**b**) Fe K-edge of Pt-Fe-N-C catalyst.

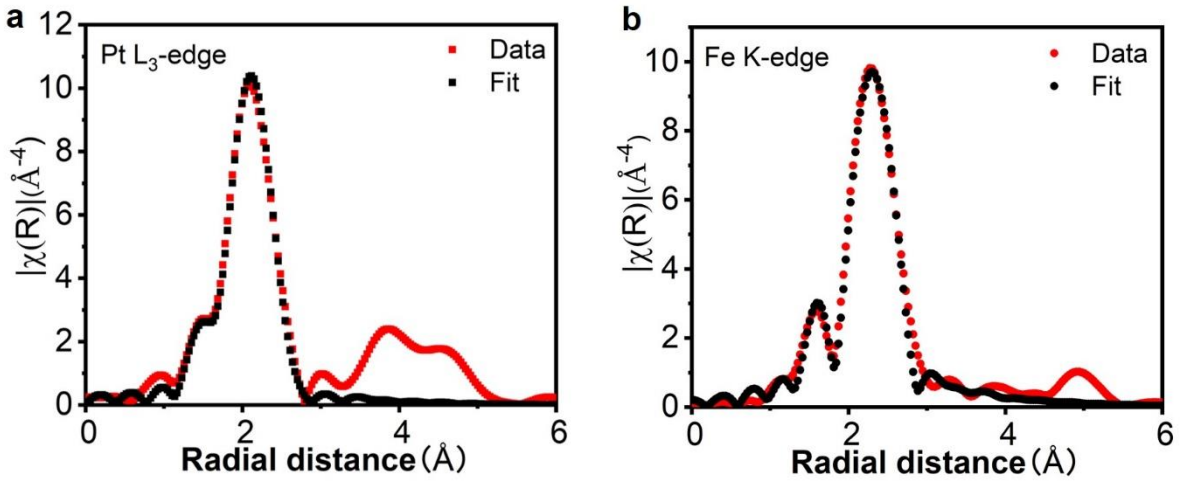

Supplementary Figure 11: EXAFS fitting in R space for (**a**) Pt L_3-edge and (**b**) Fe K-edge of Pt-Fe-N-C catalyst.

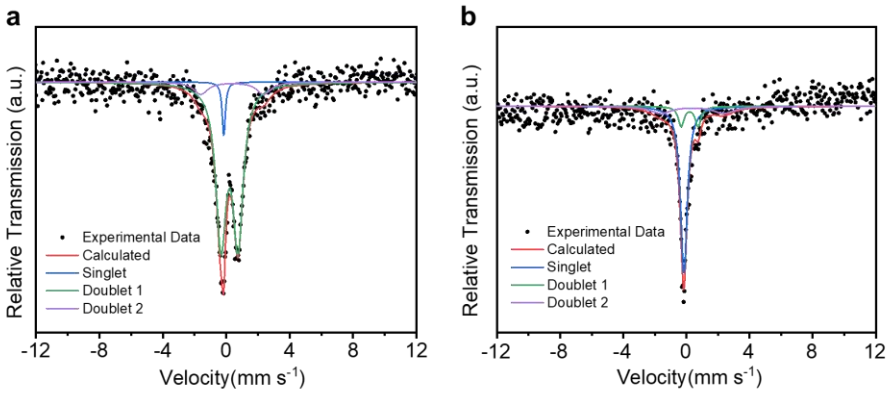

Supplementary Figure 12: ^{57}Fe Mössbauer spectroscopy characterization for (**a**) Fe-N-C and (**b**) Pt-Fe-N-C catalysts.

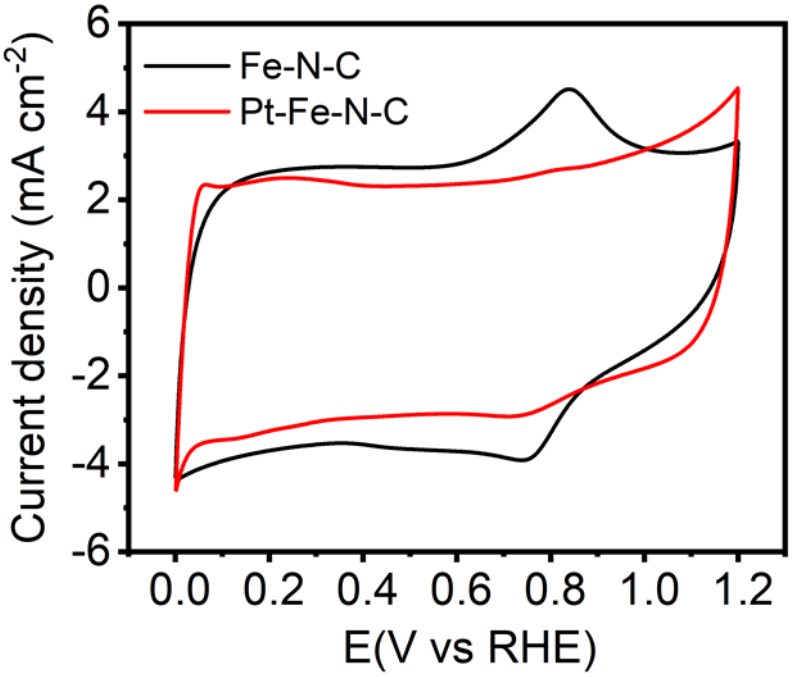

Supplementary Figure 13: Cyclic-voltammogram comparison of Pt-Fe-N-C and Fe-N-C catalysts recorded at the potential range of 0–1.2 V and 50 mV s^{-1} scan rate in an Ar-saturated 0.1 M $HClO_4$ electrolyte. The catalyst loading for Fe-N-C and Pt-Fe-N-C catalysts are both 250 ug cm^{-2}.

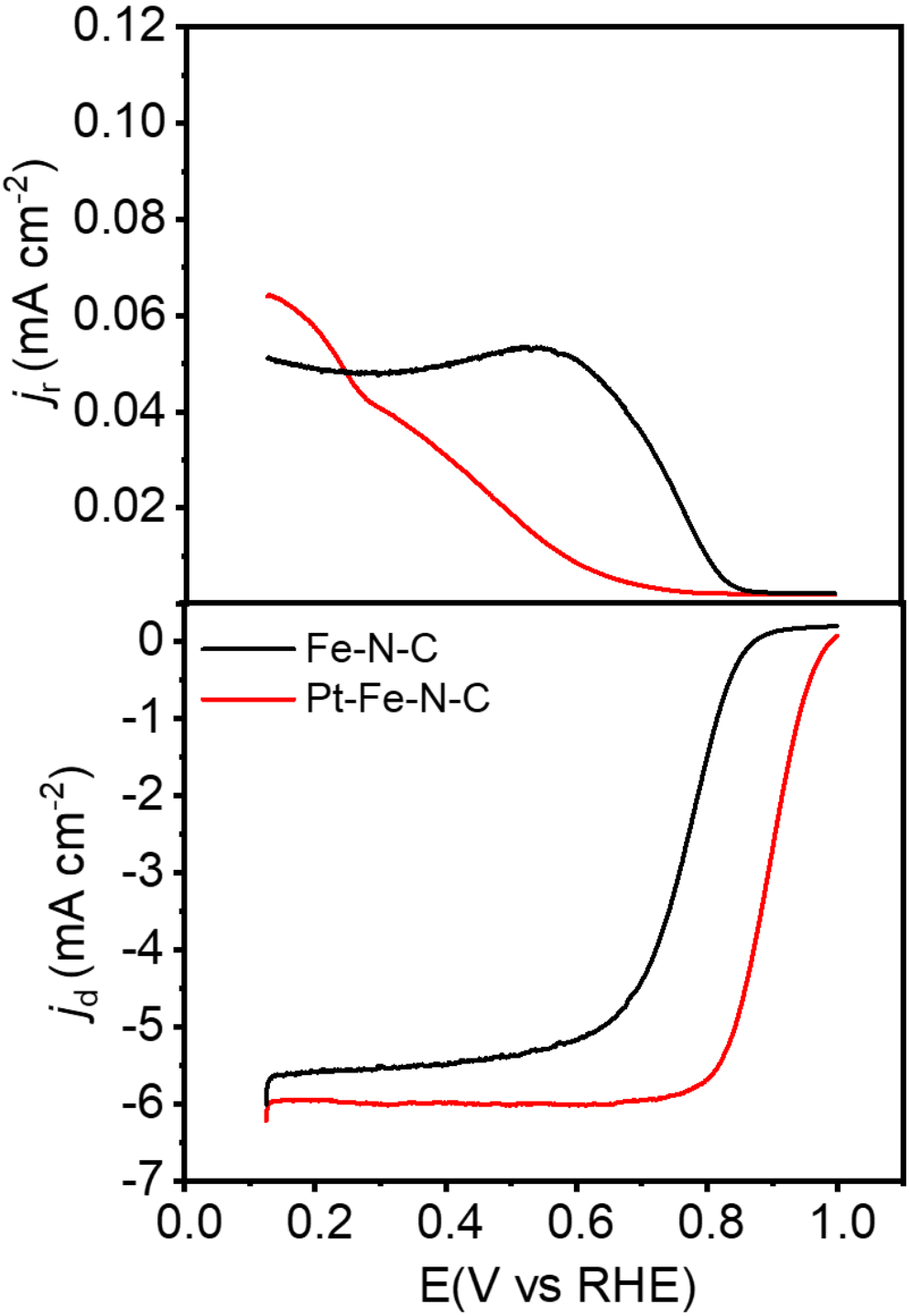

Supplementary Figure 14: Rotating-ring disk electrode responses for Pt-Fe-N-C and Fe-N-C catalysts in an O_2-saturated 0.1 M $HClO_4$ electrolyte. The disk current density (j_d) was gained by scanning the disk from 0.125 to 1.0 V and keeping the voltage of the ring at 1.2 V to record ring current density (j_r). The catalyst loading for Pt-Fe-N-C (corresponding to 4.25 μg_{Pt} cm^{-2}) and Fe-N-C are 250 ug cm^{-2}.

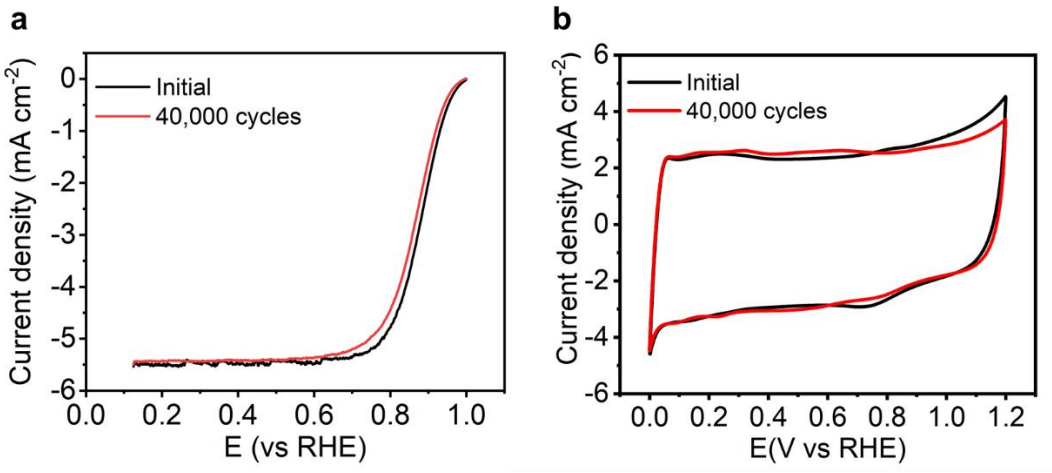

Supplementary Figure 15: (**a**) Polarization curves and (**b**) cyclic voltammograms for Pt-Fe-N-C catalyst after 40,000 cycles at the range of 0.6–1.0 V and 50 mV s^{-1} in an O_2-saturated 0.1 M $HClO_4$ electrolyte. The polarization curves were recorded from 0.125 to 1.0 V at 5 mV s^{-1} in an O_2-saturated 0.1 M $HClO_4$ electrolyte. Cyclic-voltammograms were recorded at the potential range of 0–1.2 V and 50 mV s^{-1} scan rate in an Ar-saturated 0.1 M $HClO_4$ electrolyte. The catalyst loading is 250 ug cm^{-2}.

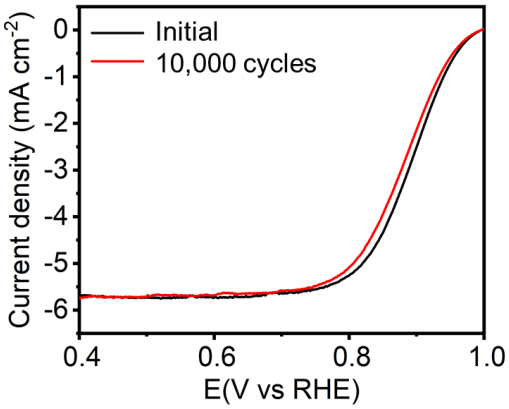

Supplementary Figure 16: Polarization curves of Pt/C catalyst before and after 10,000 cycles at 0.6–1.0 V. The polarization curves were recorded in the potential range of 0.125 to 1.0 V (shown in the range of 0.4-1.0 V for a better comparison) at 5 mV s^{-1} in an O_2-saturated 0.1 M $HClO_4$ electrolyte. The catalyst loading is 51 ug cm^{-2}.

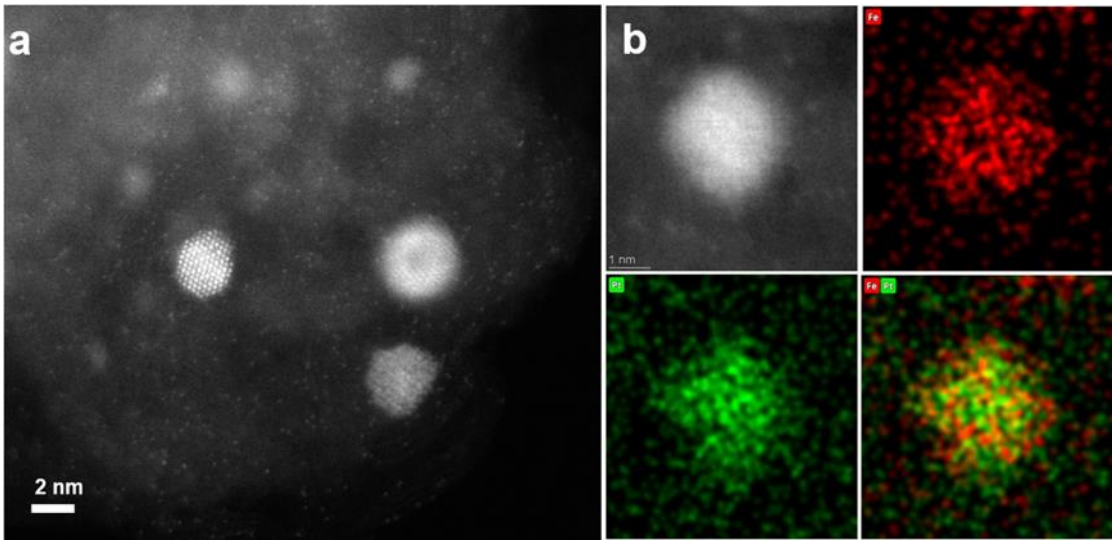

Supplementary Figure 17: (**a**) HAADF-STEM image of Pt-Fe-N-C catalyst and (**b**) EDX mapping for Fe and Pt elements after 40,000 cycles in the range of 0.6–1.0 V.

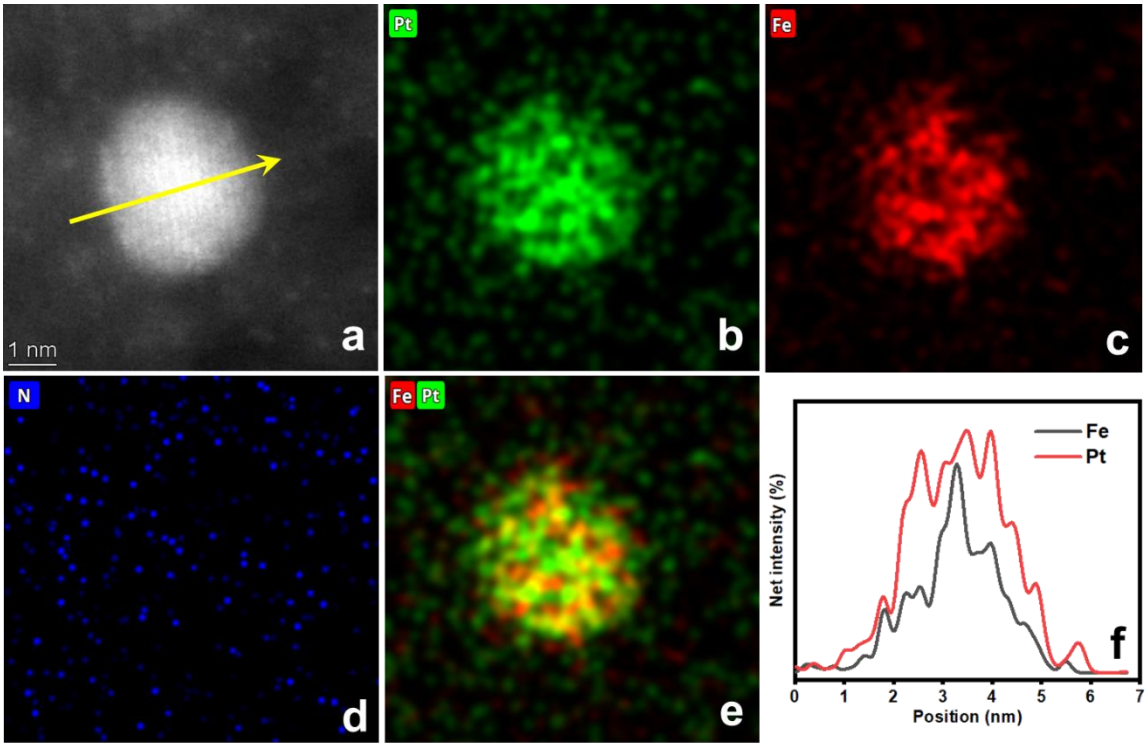

Supplementary Figure 18: (**a**) A representative nanoparticle and EDX mapping for (**b**) Pt, (**c**) Fe, (**d**) N and (**e**) Pt+Fe elements after 40,000cycles and (**f**) corresponding elemental line scan across the yellow arrow in (**a**).

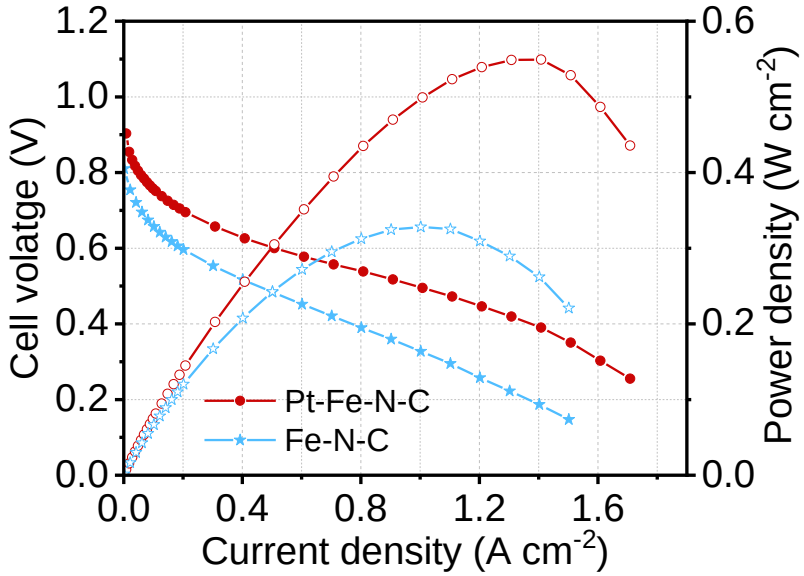

Supplementary Figure 19: H_2/air fuel cell polarization (solid symbols and left y-axis) and power density (hollow symbols and right y-axis) plots with a Pt loading of 0.015 mg_{Pt} cm^{-2} for Pt-Fe-N-C (red circles), and 3.5 mg cm^{-2} catalyst loading for Fe-N-C (blue stars) in the cathode. Membrane = Nafion HP, temperature = 80 °C, relative humidity = 100%, and anode loading = 0.1 mg_{Pt} cm^{-2}. The H_2/air fuel cell polarization curves were recorded at the H_2/air flow rates of 300/520 mL min^{-1}, absolute pressure of 1.5 bar_{anode} and 2.5 $bar_{cathode}$.

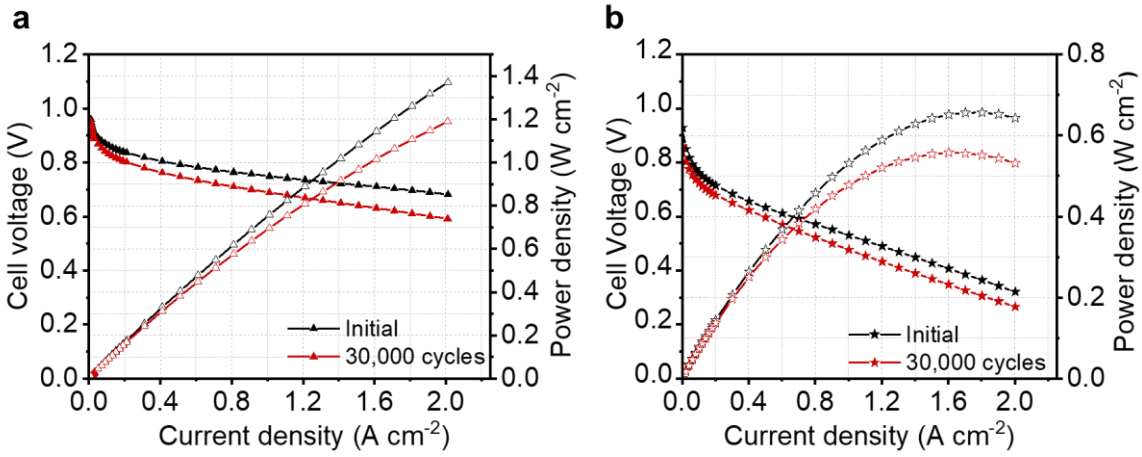

Supplementary Figure 20: (**a**) H_2/O_2 fuel cell polarization (solid symbols and left y-axis) and power density (hollow symbols and right y-axis) plots of Pt/C cathode before (black) and after (red) 30,000 voltage cycles. (**b**) H_2/O_2 fuel cell polarization (solid symbols and left y-axis) and power density (hollow symbols and right y-axis) plots of Fe-N-C cathode before (black) and after (red) 30,000 voltage cycles. Membrane = Nafion HP, temperature = 80 °C, relative humidity = 100%, and anode loading = 0.1 mg_{Pt} cm^{-2}. The H_2/O_2 fuel cell polarization curves were recorded at the H_2/O_2 flow rates of 300/300 mL min^{-1}, absolute pressure of 1.5 bar_{anode} and 2.5 $bar_{cathode}$.

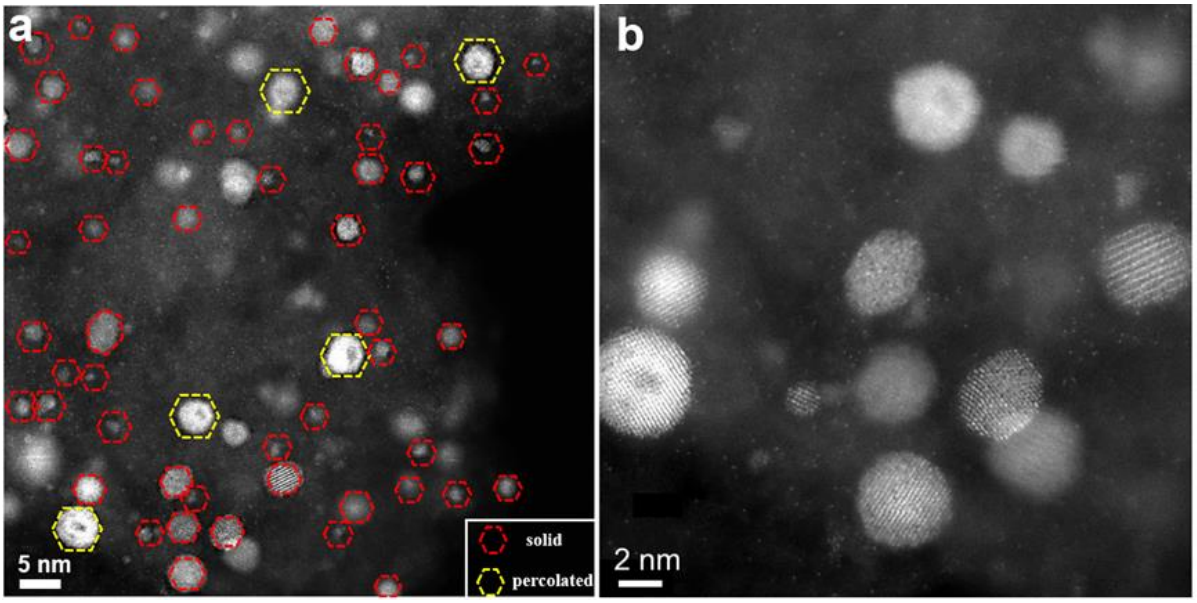

Supplementary Figure 21: HAADF-STEM image of Pt-Fe-N-C catalyst after 100,000 cycles in fuel cell.

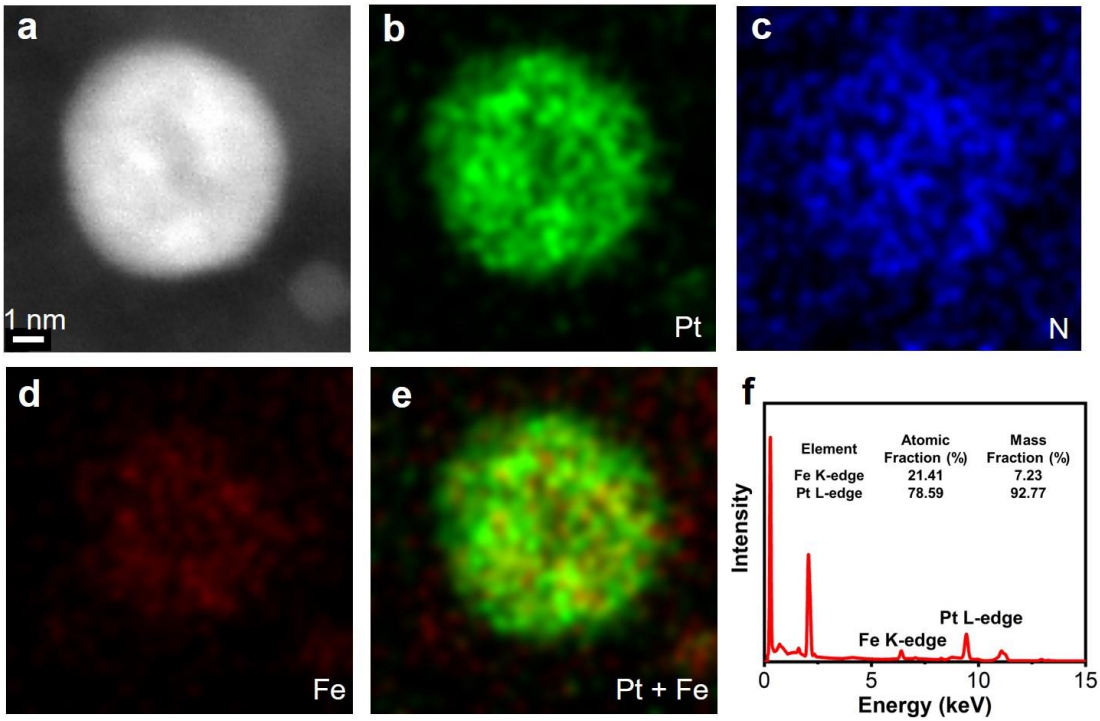

Supplementary Figure 22: (**a**) HAADF image of nanoparticle after 100,000-cycle durability test with percolated structure, and corresponding EDX mapping of (**b**) Pt, (**c**) N, (**d**) Fe, (**e**) Pt+Fe elements, and (**f**) spectrum.

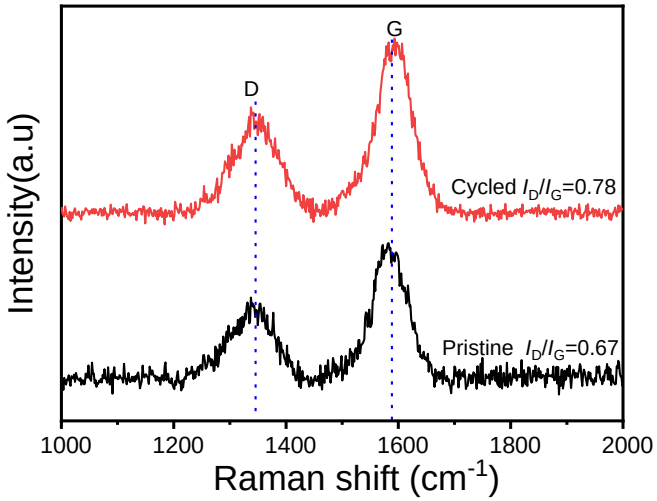

Supplementary Figure 23: Raman characterization for Pt-Fe-N-C before and after 100,000 durability cycling.

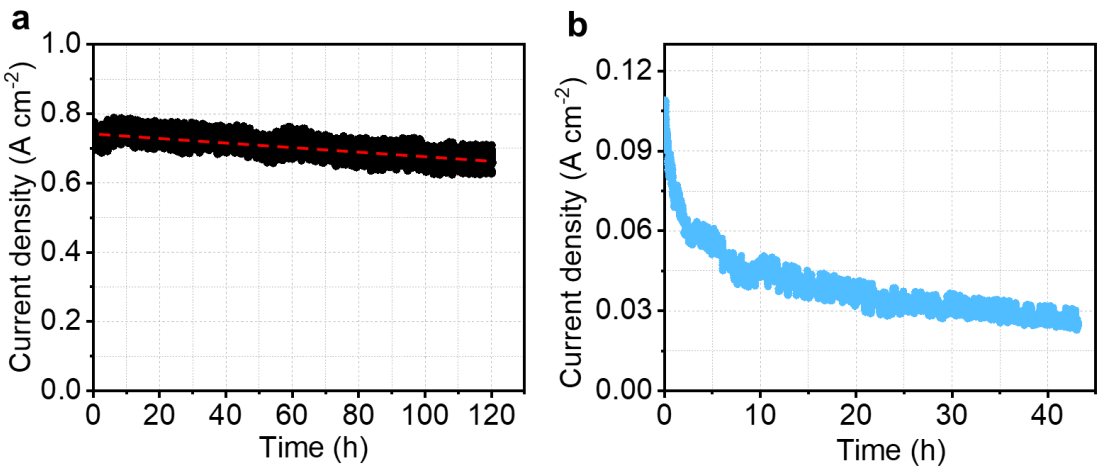

Supplementary Figure 24: Current density as a function of time for (**a**) Pt/C with 0.1 mg_{Pt} cm^{-2} loading and (**b**) Fe-N-C cathode with 3.5 mg cm^{-2} catalyst loading at potential hold durability measurement at 0.6 V in H_2/air environment. The chronoamperometric measurement at a discharge voltage of 0.6 V at H_2/air flow rates of 100/200 mL min^{-1} and1 bar absolute pressure for both anode and cathode.

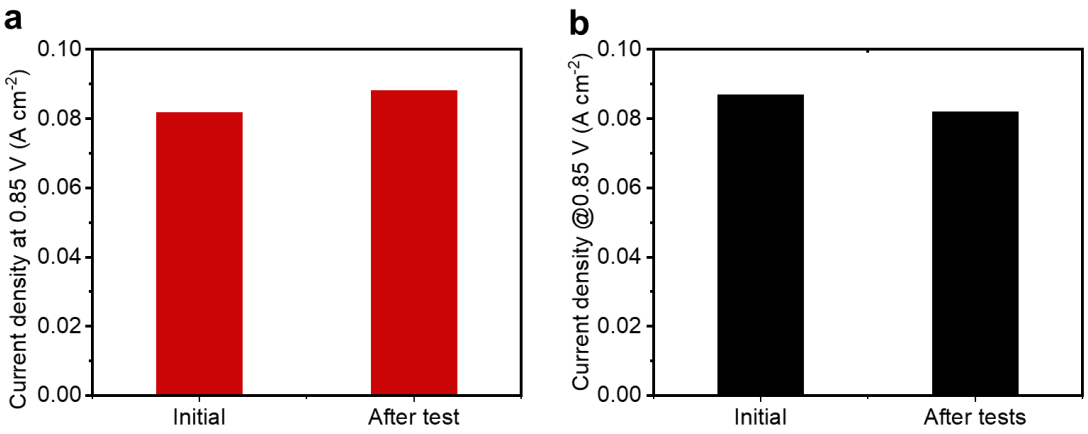

Supplementary Figure 25: The initial and final current density at 0.85 V of Pt-Fe-N-C before and after 0.6 V durability measurement in (**a**) H_2/air and (**b**) H_2/O_2 environments. The data are obtained from H_2/O_2 polarization plots.

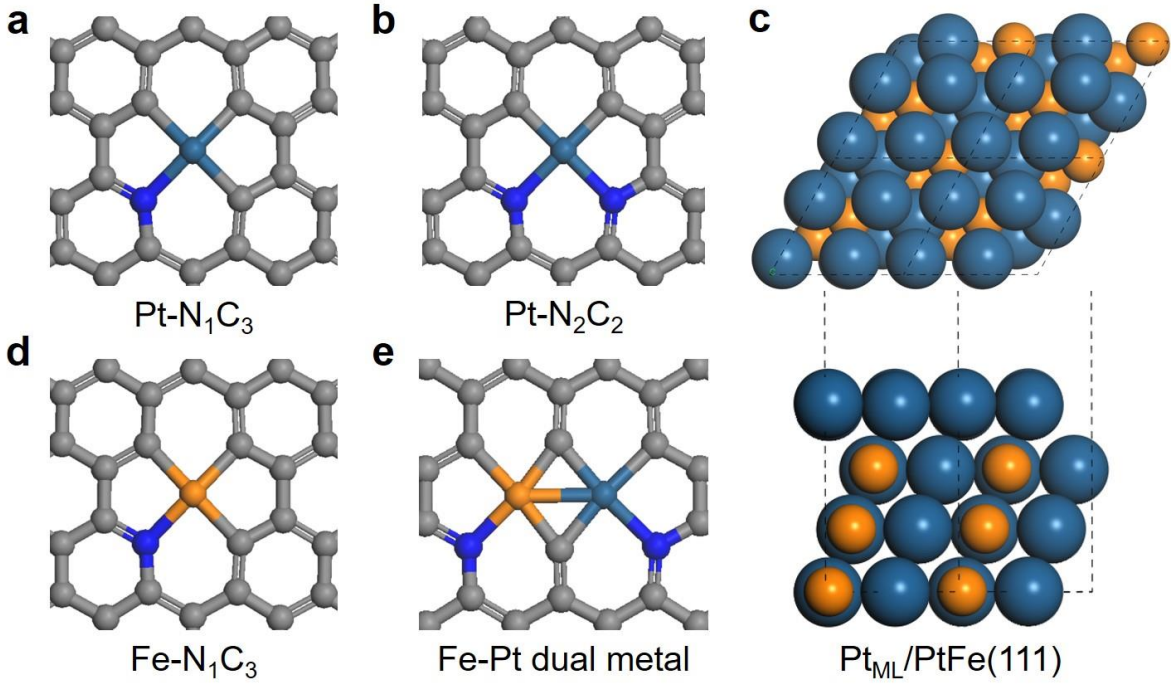

Supplementary Figure 26: Slab models for various possible active sites in Pt-Fe-N-C, including (**a**) Pt-N_1C_3, (**b**) Pt-N_2C_2, (**c**) Fe-N_1C_3, (**d**) Fe-Pt dual metal and (**e**) Pt_{ML}/PtFe(111). The dashed black line indicates the unit simulation cell. Color code: Pt: dark blue; Fe: orange; C: gray; N: blue.

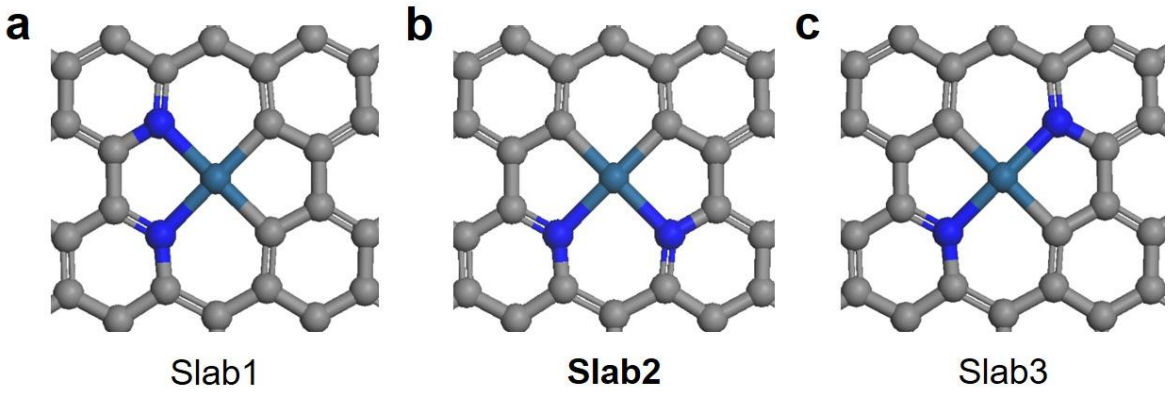

Supplementary Figure 27: Various slab models for Pt-N_2C_2. Slab2 was selected as the model catalyst for ORR pathway evaluation because it has the lowest system energy. Color code: Pt: dark blue; C: gray; N: blue.

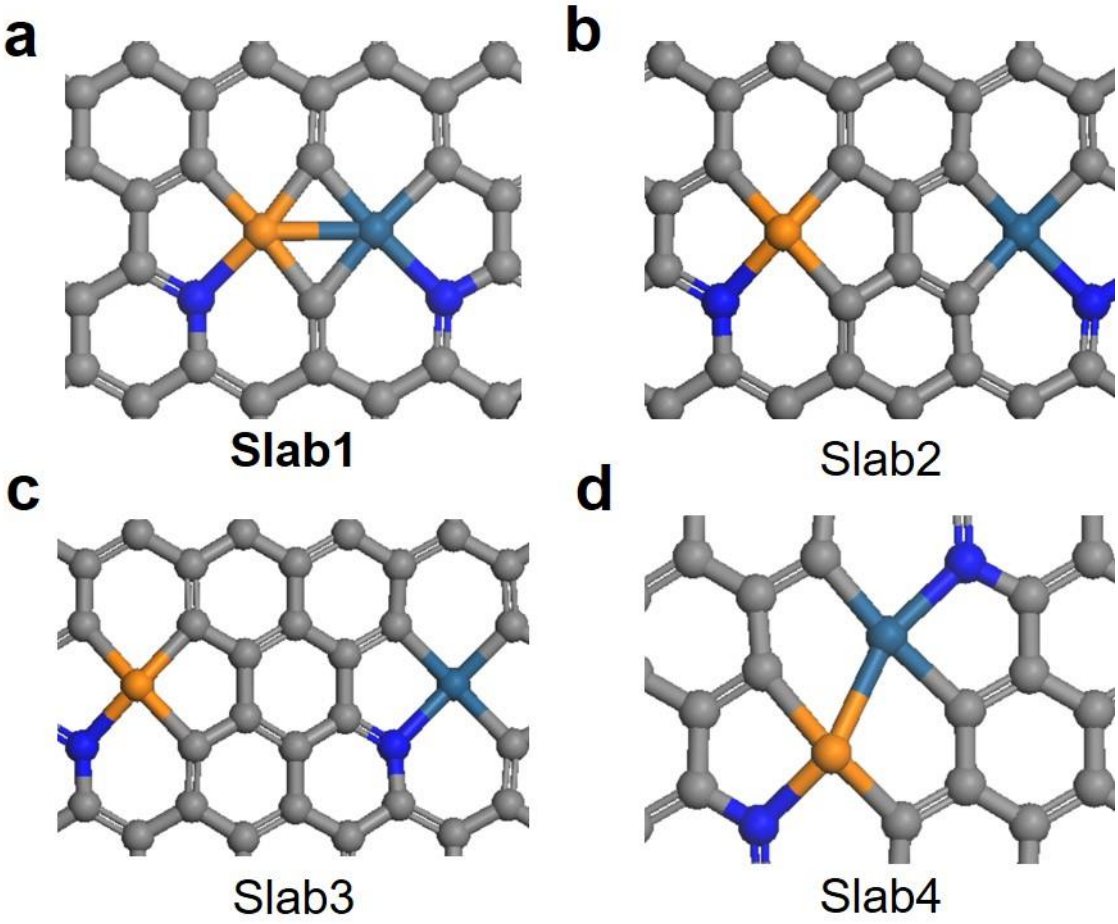

Supplementary Figure 28: Various slab models for Fe-Pt dual metal. Slab1 was selected as the model catalyst for ORR pathway evaluation because it has the lowest system energy. Color code: Pt: dark blue; Fe: orange; C: gray; N: blue.

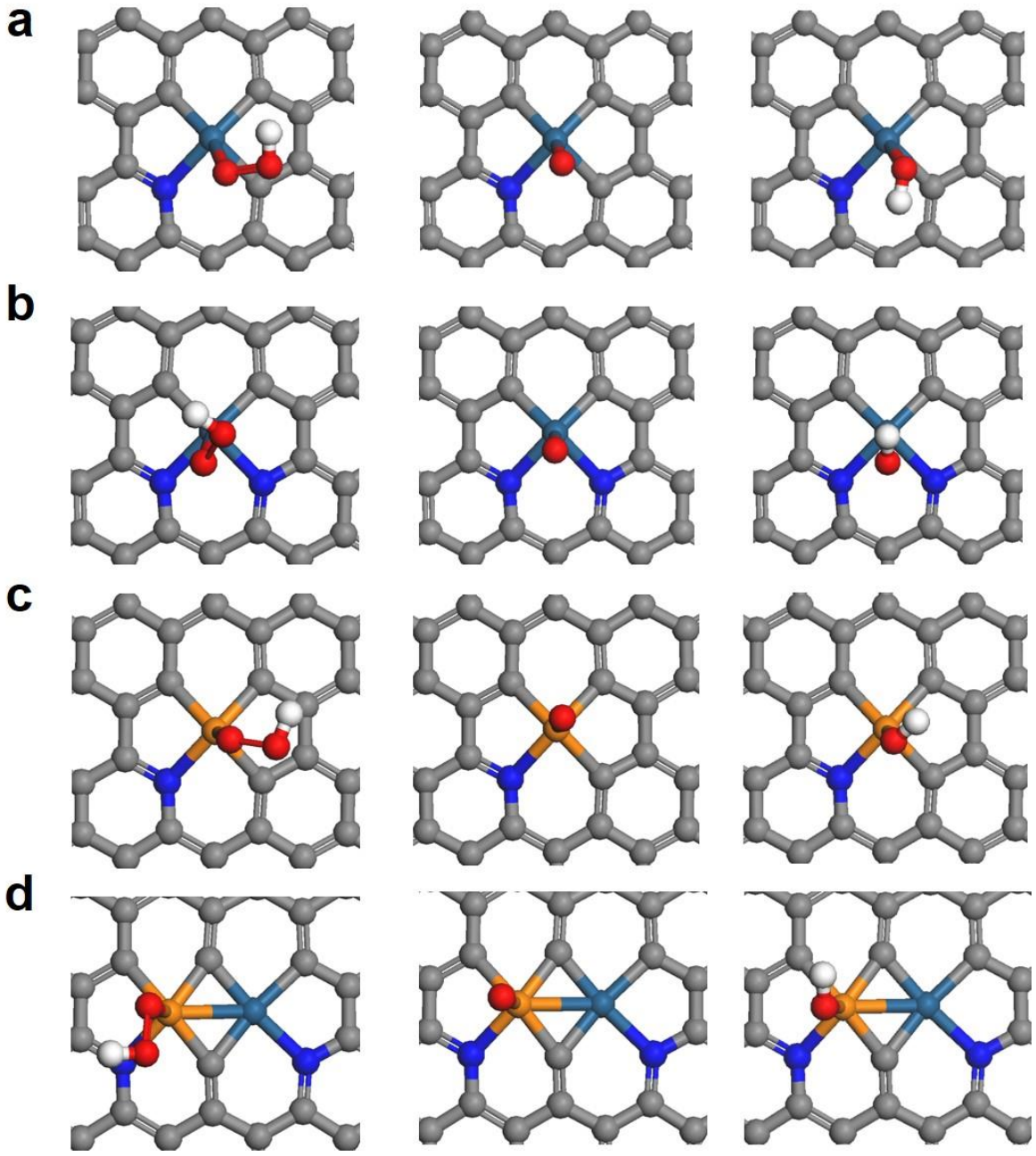

Supplementary 29: Optimized adsorption structures of *OOH, *O and *OH on (**a**) Pt-N_1C_3, (**b**) Pt-N_2C_2, (**c**) Fe-N_1C_3 and (**d**) Fe-Pt dual metal. Color code: Pt: dark blue; Fe: orange; C: gray; N: blue; O: red; H: white.

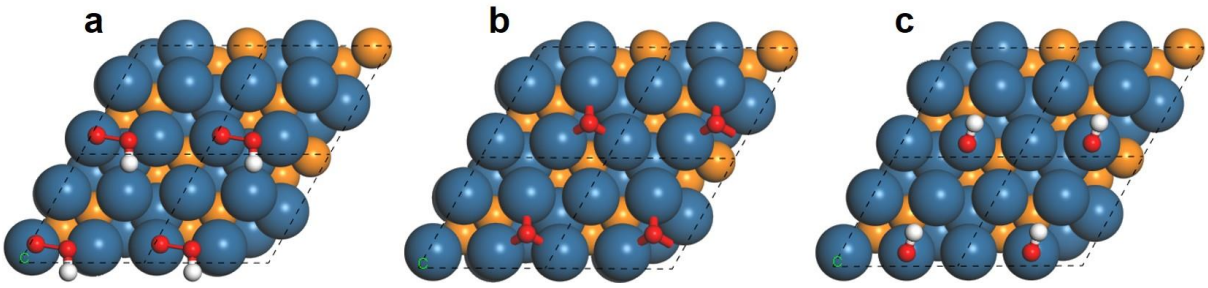

Supplementary Figure 30: Optimized adsorption structures of (**a**) *OOH, (**b**) *O and (**c**) *OH on Pt_{ML}/PtFe(111). The structures of (4 × 4) supercells are shown, and the coverage of adsorbates is 0.25 ML. Color code: Pt: dark blue; Fe: orange; O: red; H: white.

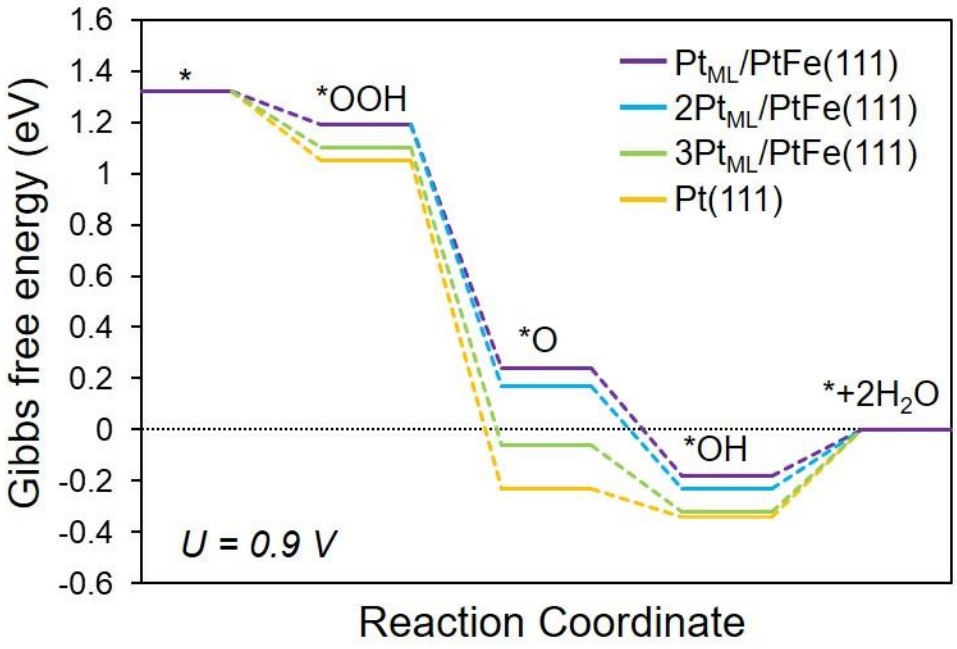

Supplementary Figure 31: Gibbs free energy diagram of ORR on core-shell nanoparticles with various numbers of layers of Pt skin at U = 0.9 V, including Pt_{ML}/PtFe(111), $2Pt_{ML}$/PtFe(111), and $3Pt_{ML}$/PtFe(111). The free energy curve of Pt(111) is also shown for comparison.

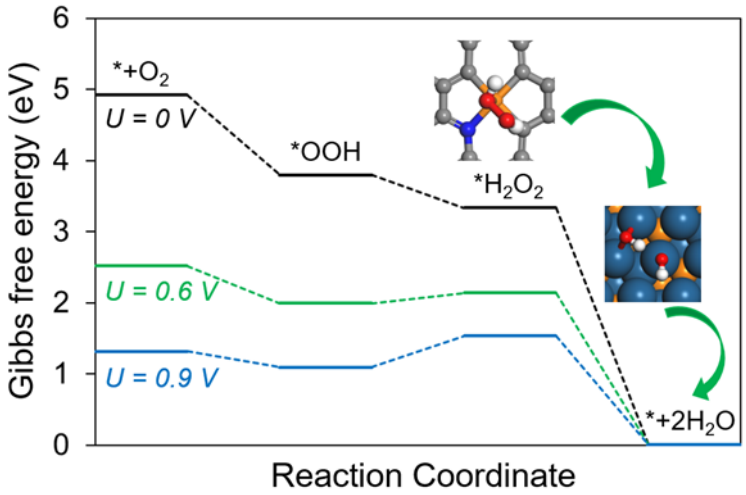

Supplementary Figure 32: Gibbs free energy diagram of H_2O_2 formation on Fe-N_1C_3 and H_2O_2 reduction on Pt_{ML}/PtFe(111). Color code: Pt: dark blue; Fe: orange; C, grey; N: blue; O: red; H: white.

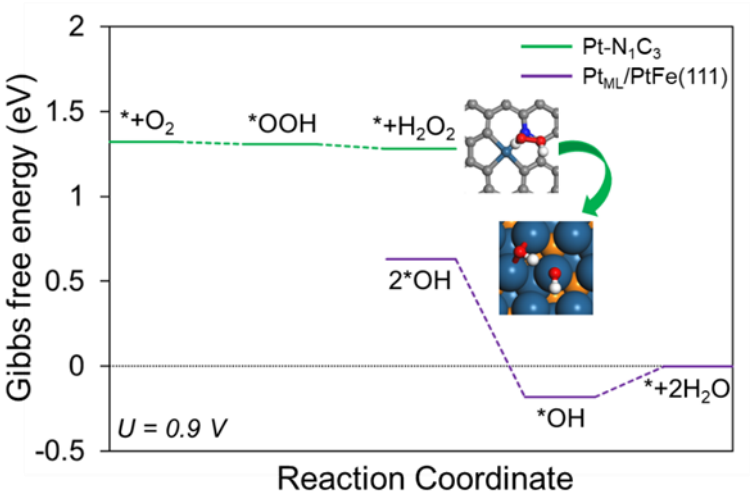

Supplementary Figure 33: Gibbs free energy diagram of H_2O_2 formation on Pt-N_1C_3 and H_2O_2 reduction on Pt_{ML}/PtFe(111) at U = 0.9 V. Color code: Pt: dark blue; Fe: orange; N: blue; O: red; H: white.

Supplementary Table 1: Fitting parameters of Pt L_3-edge and Fe K-edge EXAFS spectra of Pt-Fe-N-C catalyst. (N: coordination number; R: distance between absorber and backscatter atoms; σ^2: the Debye–Waller factor value.)

Spectrum	Model	Element	N	R(Å)	σ^2 (10^{-3} Å^2)
Pt L_3-edge	1	C/N/O	1/2	2.01±0.033	12±4
	2	Fe	4	2.64±0.009	4±1
Fe K-edge	1	C/N/O	1	1.94±0.031	8±4
	2	Fe	5	2.53±0.005	9±1
	3	Pt	1	2.65±0.045	8±4

This EXAFS fitting result is the reference for single atom model setting during DFT calculation. Metal-O is arisen from the adsorption bond between metal and O_2, which is observable for catalyst exposed to air and is unstable during reaction. Thus, metal-N was put into the consideration and the total coordination number was proposed to four based on the previous experience.[2,3]

Supplementary Table 2: Mössbauer parameters derived from the fittings. Isomer shift (IS), quadrupole splitting (QS), line width (Γ) and relative spectral area % of each component.

Materials	Component	IS (mm/s)	QS (mm/s)	Γ (mm/s)	Area (%)	Assignment
Fe-N-C	Singlet	-0.16	—	0.24	4.7	γ-Fe
	Doublet1	0.20	1.07	0.77	85.9	$FeN_4(Fe^{II},LS)$
	Doublet2	0.38	3.97	1.09	9.5	$FeN_4(Fe^{II},MS)$
Pt-Fe-N-C	Singlet	-0.16	—	0.51	68.0	largely from Pt-Fe alloy
	Doublet1	0.20	1.07	0.44	13.9	$FeN_4(Fe^{II},LS)$
	Doublet2	0.38	3.97	1.58	18.0	$FeN_4(Fe^{II},MS)$

Supplementary Table 3: Summary ORR performance of reported Pt-based electrodes.

Catalyst *(ref.)*	MA[a] in LC[b] ($A\ mg^{-1}$)	MA in FC[c] ($A\ mg^{-1}$)	Pt loading in cathode ($mg\ cm^{-2}$)	Power density ($W\ cm^{-2}$) /current density ($A\ cm^{-2}$)	Durability (in FC)
Pt-Fe-N-C This work	1.74	0.77[¶]	0.015	1.08/2	3% MA loss after 100,000 cycles No current drop at 0.6 V over 200h in both H_2/air and H_2/O_2 in FC
PtNi nanocage/C [4]	3.52	Not given	0.15	Not given	3% current density decay at 0.6 V after 180 h in H_2/air
fct-PtFe/C [5]	1.60	-	$0.2_{(Pt+Fe)}$	0.52* /1.2	3.4% PPD[d] drop after 100 h polarization tests
W-doped $L1_0$-CoPt [6]	2.21	0.57	0.11	Not given	17.5% MA loss after 30,000 cycles
Connected PtFe [7]	0.53*	-	0.3	0.62*/1	Negligible performance loss after 10,000 cycles
$L1_0$-CoPt@Pt/C [8]	2.26	0.56	0.105	Not given	19% MA loss after 30,000 cycles
PtCo@Pt/C [9]	0.335	0.105	0.2	1.287/2.7*	25% PPD decay after 30,000 cycles
PtNi nanocage/C [10]	0.501	Not given	0.1	1.28/Not given	58% MA loss after 30,000 cycles

Catalyst *(ref.)*	MA[a] in LC[b] ($A\ mg^{-1}$)	MA in FC[c] ($A\ mg^{-1}$)	Pt loading in cathode ($mg\ cm^{-2}$)	Power density ($W\ cm^{-2}$) /current density ($A\ cm^{-2}$)	Durability (in FC)
$L1_0$-PtZn [11]	1.02	0.52	0.10	1.25*/2	16.6% MA loss after 30,000 cycles
PtNiCo/NC [12]	7.21	Not given	0.12	1.07/2.2*	Negligible PPD decay after 100 h in H_2/O_2
cBCP-PtFe [13]	9.0	0.81/0.26[¶]	0.01	0.98/2.6*	30.6% PPD loss after 30,000 cycles
Pt–Ni–Au /C [14]	0.651	Not given	0.1	0.55/1.2*	27.3% current density (0.6 V) decay after 10,000 cycles
PtNi@Pt/C [15]	1.24	Not given	0.2	2.4/5*	37.5% PPD decay after 30,000 cycles
Pt/N-KB 600°C[16]	0.35	0.20[¶]	0.11	1.39/2.5*	Negligible performance loss after 1500 cycles
Pt/carbon coated TiO_2 [17]	0.92	Not given	0.15	1.07/2.5*	23.4% current density (0.6 V) decay after 10,000 cycles

[a]MA: mass activity at 0.9 V. [b]LC: liquid cell. [c]FC: fuel cell. *The data are not given directly in some studies but are extracted from the fuel-cell polarization curves. [d]PPD: peak power density. [¶]The mass activity is calculated at 1 bar absolute pressure of H_2 and O_2.

Supplementary Table 4: Summary ORR performance of hybrid electrocatalysts.

Catalyst *(ref.)*	Pt loading of catalyst (Wt.%)	MA[a] in LC[b] ($A\ mg^{-1}$)	MA in FC[c] ($A\ mg^{-1}$)	ML[d]/PD[e]/CD[f] ($mg_{Pt}\ cm^{-2}$/$W\ cm^{-2}$/ $A\ cm^{-2}$)	Durability (LC or FC)
Pt-Fe-N-C (This work)	1.7	1.74	0.77[¶]	0.015/1.08/2	14 mV $E_{1/2}$ loss after 40,000 cycles in LC 3% MA loss after 100,000 cycles in FC No current drop at 0.6 V over 200h in both H_2/air and H_2/O_2 in FC
Pt-Co/Co-N-C(LP@PF-1) **[18]**	2.72	8.64	1.08/0.65[¶]	0.033/1.05*/2	36% MA loss after 30,000 cycles in FC
Pt-Co/Co-N-C(LP@PF-2) **[18]**	2.81	12.36	1.77/1.07[¶]	0.035/1.2*/2	85% MA loss after 30,000 cycles in FC
$Pt_A@Fe_{SA}$-N-C **[19]**	13.1	Not given	0.45	0.13/1.31/2.81	24.4% current density (0.6 V) drop after 10,000 cycles in FC
Pt/FeN_4-C**[20]**	20	0.57	0.45	0.1/1.31*[Δ]/1.5	20% MA loss after 30,000 cycles in FC
Pt_3Co/ FeN_4-C**[20]**	20	1.34	0.72	0.1/0.88*[Δ]/1.5	38% MA loss after 30,000 cycles in FC
Pt_3Co/Co-N-C**[21]**	20	1.15 (SA^g)	Not given	0.13/0.70*[Δ]/1.3	12 mV $E_{1/2}$ loss after 30,000 cycles in LC
Pt/ZnFe-N-C**[22]**	2.4	0.22	Not given	0.035/1.02/2.5	1 mV $E_{1/2}$ loss after 2,000 cycles in LC

Catalyst *(ref.)*	Pt loading of catalyst (Wt.%)	MA[a] in LC[b] (A mg^{-1})	MA in FC[c] (A mg^{-1})	ML[d]/PD[e]/CD[f] (mg_{Pt} cm^{-2}/W cm^{-2}/ A cm^{-2})	Durability (LC or FC)
Pt–FeNC[23]	2.1 (μg cm^{-2})	0.69 (initial)	Not given	Not given	23% MA rise after 25,000 cycles in LC
Pt/Fe-N-C[24] ($Pt_{2.0}Fe_{1.0}d$)	1.7	Similar activity as Fe-N-C			Stable current density at 0.5 V for 180 h in FC
Pt/Fe-N-C[25] (Pt5/FeNC)	5	2.19	$18.76_{@0.6V}$	0.18/0.8* /2	-
Pt/C_Fe/N/C[26] (0.035_{Pt}_1.0 mg cm^{-2})	0.035 (mg cm^{-2})	Not given	0.22	0.035/0.63* /1.4	11%* current density loss at 0.6 V for 100 h in FC
CoN-Pt/CoNC-2D[27]	23.68	Not given	2.14@0.8V	0.1/1.33/3*	17 mV $E_{1/2}$ loss after 30,000 cycles in LC; 12.1% MA (0.8 V) loss after 100 h at 1.0 A cm^{-2} in FC
L-Co-doped Pt/CCC [28]	30	Not given	0.47	0.1/1.05 [Δ] /1.8	66% MA loss at after 30, 000in FC

[a]MA: mass activity at 0.9 V (except for special mark). [b]LC: liquid cell. [c]FC: fuel cell. [d]ML:Pt mass loading in the cathode. [e]PD: power density. [f]CD: current density for reading the power density. [g]SA: specific activity (mA cm_{Pt}^{-2}) at 0.9 V. [h]PPD: peak power density. *The data are not given directly in some studies but are extracted from the fuel-cell polarization curves. [Δ]The fuel cell data recorded in H_2/air environment. [¶]The mass activity is calculated at 1 bar absolute pressure of H_2 and O_2.

Supplementary Table 5: DFT calculated energy for various slab models for Pt-N_2C_2 and Fe-Pt dual metal. The unit is eV.

	Slab1	Slab2	Slab3	Slab4
Pt-N_2C_2	-653.44	**-653.78**	-653.21	N/A
Fe-Pt dual metal	**-637.56**	-634.52	-634.65	-636.97

Supplementary Table 6: Gibbs free energies of key intermediates in the free energy diagram of ORR on various possible active sites at U = 0.9 V. The unit is eV.

	*OOH	*O	*OH
Pt-N_1C_3	1.31	1.07	**-0.17**
Pt-N_2C_2	**1.86**	1.85	0.55
Fe-N_1C_3	1.10	0.28	**-0.53**
Fe-Pt dual metal	1.04	0.30	**-0.75**
Pt_{ML}/PtFe(111)	1.19	0.24	**-0.18**
Pt(111)	1.05	-0.23	**-0.34**

The bold numbers represent the key intermediates determining the energy barriers, and all of the active sites show the energy barriers in the last *OH-to-H_2O step except for the Pt-N_2C_2, where *OOH formation is the most difficult step, with an energy barrier of 0.54 eV. It should be noted that the energy levels of *OOH and *OH were corrected by -0.48 eV and -0.575 eV, respectively, with the consideration of solvation effects.[29]

Supplementary Table 7: Gibbs free energies of key intermediates in the free energy diagram of H_2O_2 reduction reaction on Pt_{ML}/PtFe(111) and Pt(111) at U = 0.9 V. The unit is eV.

	2*OH	*OH
Pt_{ML}/PtFe(111)	0.63	-0.18
Pt(111)	0.19	-0.34

Supplementary References

1 Xiao, F. *et al.* Nitrogen-coordinated single iron atom catalysts derived from metal organic frameworks for oxygen reduction reaction. *Nano Energy* **61**, 60-68 (2019).

2 Zhang, H. *et al.* Single Atomic Iron Catalysts for Oxygen Reduction in Acidic Media: Particle Size Control and Thermal Activation. *J. Am. Chem. Soc.* **139**, 14143-14149 (2017).

3 Liu, K., Wu, G. & Wang, G. Role of local carbon structure surrounding FeN4 sites in boosting the catalytic activity for oxygen reduction. *J. Phys. Chem. C* **121**, 11319-11324 (2017).

4 Tian, X. *et al.* Engineering bunched Pt-Ni alloy nanocages for efficient oxygen reduction in practical fuel cells. *Science* **366**, 850–856 (2019).

5 Chung, D. Y. *et al.* Highly Durable and Active PtFe Nanocatalyst for Electrochemical Oxygen Reduction Reaction. *J. Am. Chem. Soc.* **137**, 15478–15485 (2015).

6 Liang, J. *et al.* Tungsten-Doped $L1_0$-PtCo Ultrasmall Nanoparticles as a High‐Performance Fuel Cell Cathode. *Angew. Chem. Int. Ed.* **58**, 15471–15477 (2019).

7 Tamaki, T. *et al.* Connected nanoparticle catalysts possessing a porous, hollow capsule structure as carbon-free electrocatalysts for oxygen reduction in polymer electrolyte fuel cells. *Energy Environ. Sci.* **8**, 3545–3549 (2015).

8 Li, J. *et al.* Hard-Magnet $L1_0$-CoPt Nanoparticles Advance Fuel Cell Catalysis. *Joule* **3**, 124–135 (2019).

9 Lee, S. *et al.* Development of robust Pt shell through organic hydride donor in PtCo@Pt core-shell electrocatalysts for highly stable proton exchange membrane fuel cells. *J.Catal.* **379**, 112–120 (2019).

10 Peng, X., Zhao, S., Omasta, T. J., Roller, J. M. & Mustain, W. E. Activity and durability of Pt-Ni nanocage electocatalysts in proton exchange membrane fuel cells. *Appl. Catal. B* **203**, 927–935 (2017).

11 Liang, J. *et al.* Biaxial Strains Mediated Oxygen Reduction Electrocatalysis on Fenton Reaction Resistant $L1_0$-PtZn Fuel Cell Cathode. *Adv. Energy Mater.* **10**, 2000179 (2020).

12 Hanif, S. *et al.* ZIF derived PtNiCo/NC cathode catalyst for proton exchange membrane fuel cell. *Appl. Catal. B* **258**, 117947 (2019).

13 Choi, J. *et al.* Highly durable fuel cell catalysts using crosslinkable block copolymer-based carbon supports with ultralow Pt loadings. *Energy Environ. Sci.* **13**, 4921–4929 (2020).

14 Lin, Z. *et al.* Ternary heterogeneous Pt–Ni–Au nanowires with enhanced activity and stability for PEMFCs. *ChemComm* **56**, 4276–4279 (2020).

15 Choi, J. *et al.* Gram-scale synthesis of highly active and durable octahedral PtNi nanoparticle catalysts for proton exchange membrane fuel cell. *Appl. Catal. B* **225**, 530–537 (2018).

16 Ott, S. *et al.* Ionomer distribution control in porous carbon-supported catalyst layers for high-power and low Pt-loaded proton exchange membrane fuel cells. *Nat. Mater.* **19**, 77–85 (2020).

17 Dhanasekaran, P., Selvaganesh, S. V., Shukla, A., Nagaraju, N. & Bhat, S. D. Boosting Pt oxygen reduction reaction activity and durability by carbon semi-coated titania nanorods for proton exchange membrane fuel cells. *Electrochim. Acta* **263**, 596–609 (2018).

18 Chong, L. *et al.* Ultralow-loading platinum-cobalt fuel cell catalysts derived from imidazolate frameworks. *Science* **362**, 1276–1281 (2018).

19 Ao, X. *et al.* Atomically dispersed Fe–N–C decorated with Pt-alloy core–shell nanoparticles for improved activity and durability towards oxygen reduction. *Energy Environ. Sci.* **13**, 3032–3040 (2020).

20 Qiao, Z. *et al.* Atomically dispersed single iron sites for promoting Pt and Pt_3Co fuel cell catalysts: performance and durability improvements. *Energy Environ. Sci.* **14**, 4948-4960 (2021).

21 Wang, X. X. *et al.* Ordered Pt_3Co Intermetallic Nanoparticles Derived from Metal–Organic Frameworks for Oxygen Reduction. *Nano Lett.* **18**, 4163–4171 (2018).

22 Li, J. *et al.* Cross-linked multi-atom Pt catalyst for highly efficient oxygen reduction catalysis. *Appl. Catal. B* **284**, 119728 (2021).
23 Kuttiyiel, K. A. *et al.* Janus structured Pt–FeNC nanoparticles as a catalyst for the oxygen reduction reaction. *ChemComm* **53**, 1660-1663 (2017).
24 Mechler, A. K. *et al.* Stabilization of Iron-Based Fuel Cell Catalysts by Non-Catalytic Platinum. *J. Electrochem. Soc.* **165**, F1084 (2018).
25 Park, J.-Y. *et al.* Enhanced oxygen reduction reaction of Pt deposited Fe/N-doped bimodal porous carbon nanostructure catalysts. *J.Catal.* **359**, 46-54 (2018).
26 Yang, X. *et al.* PGM-Free Fe/N/C and Ultralow Loading Pt/C Hybrid Cathode Catalysts with Enhanced Stability and Activity in PEM Fuel Cells. *ACS Appl. Mater. Interfaces* **12**, 13739-13749 (2020).
27 Tran, T.-N. *et al.* Synergistic CoN-Decorated Pt Catalyst on Two-Dimensional Porous Co–N-Doped Carbon Nanosheet for Enhanced Oxygen Reduction Activity and Durability. *ACS Appl. Energ. Mater.* **3**, 6310-6322 (2020).
28 Xie, T., Jung, W., Kim, T., Ganesan, P. & Popov, B. N. Development of Highly Active and Durable Hybrid Cathode Catalysts for Polymer Electrolyte Membrane Fuel Cells. *J. Electrochem. Soc.* **161**, F1489 (2014).
29 Calle-Vallejo, F. *et al.* Finding optimal surface sites on heterogeneous catalysts by counting nearest neighbors. *Science* **350**, 185–189 (2015).